

Evidence for large-scale climate forcing of dense shelf water variability in the Ross Sea

Received: 21 November 2023

Accepted: 11 September 2024

Published online: 18 September 2024

 Check for updates

Zhaoru Zhang ^{1,2,3,4}✉, Chuan Xie ¹, Pasquale Castagno⁵,
Matthew H. England ⁶, Xiaoqiao Wang¹, Michael S. Dinniman ⁷,
Alessandro Silvano ⁸, Chuning Wang¹, Lei Zhou ¹, Xichen Li ⁹,
Meng Zhou^{1,2,3,4} & Giorgio Budillon¹⁰

Antarctic Bottom Water (AABW), which supplies the lower limb of the thermohaline circulation, originates from dense shelf water (DSW) forming in Antarctic polynyas. Here, combining a long mooring record of DSW measurements with numerical simulations and satellite data, we show that significant correlation exists between interannual variability of DSW production in the Ross Sea polynyas, where DSW contributes between 20–40% of the global AABW production, and the Southern Annular Mode (SAM). The correlation is largest when the Amundsen Sea Low (ASL) is weakened and shifted east of the Ross Sea. During positive SAM phases, enhanced offshore winds and lower air temperatures over the western Ross Sea increase sea ice production and promote DSW formation, with the opposite response during negative SAM phases. These processes ultimately modulate AABW thickness in the open ocean. A projected positive shift of the SAM and eastward displacement of the ASL thus has implications for the future of DSW and AABW formation.

Dense shelf water (DSW) formed by convective processes on Antarctic continental shelves, mainly from polynyas defined as low sea-ice-concentration areas, is the major source of the Antarctic Bottom Water (AABW)^{1–5}, which feeds the lower limb of the global thermohaline circulation^{6–8}. The formation and transport of DSW and AABW play an important role in transporting carbon from the biologically productive polynyas to the deep ocean^{9,10}. Polynyas along the Antarctic coast are formed by cold katabatic winds blowing off the Antarctic continent toward the ocean, which drives sea ice transport offshore^{11–14}. As the warm ocean is in direct contact with the cold air, massive heat loss leads to high sea ice production rates^{15,16} and drives the formation of

the DSW via brine release and ocean convection^{5,17}. The DSW is subsequently transported towards the shelf break and flows down the continental slope as gravity plumes^{18,19}, entraining the Circumpolar Deep Water (CDW) to ultimately form AABW.

The Ross Sea is responsible for 20–40% of the total AABW production^{20,21}, and the Terra Nova Bay polynya (TNBP) off the Victoria Land coast and the Ross Ice Shelf polynya (RISP) (Fig. 1a, b) are the two major formation sites of DSW in the Ross Sea²². The TNBP is opened by strong katabatic winds flowing eastward from the Transantarctic Mountains¹¹, and RISP is maintained by offshore winds off the Ross Ice Shelf contributed by confluent drainage flows from West Antarctic ice

¹Key Laboratory of Polar Ecosystem and Climate Change, Ministry of Education and School of Oceanography, Shanghai Jiao Tong University, Shanghai, China.

²Shanghai Key Laboratory of Polar Life and Environment Sciences, Shanghai Jiao Tong University, Shanghai, China. ³Shanghai Frontiers Science Center of Polar Science, Shanghai Jiao Tong University, Shanghai, China. ⁴Key Laboratory for Polar Science, Polar Research Institute of China, Ministry of Natural Resources, Shanghai, China. ⁵Department of Mathematical Sciences and Informatics, Physics and Earth Sciences, University of Messina, Messina, Italy.

⁶Centre for Marine Science and Innovation (CMSI) and Australian Centre for Excellence in Antarctic Science, University of New South Wales, Sydney, NSW, Australia. ⁷Center for Coastal Physical Oceanography, Old Dominion University, Norfolk, VA, USA. ⁸Ocean and Earth Science, National Oceanography Centre, University of Southampton, Southampton, UK. ⁹Institute of Atmospheric Physics, Chinese Academy of Sciences, Beijing, China. ¹⁰Department of Sciences and Technologies, Parthenope University, Naples, Italy. ✉e-mail: zrzhang@sjtu.edu.cn

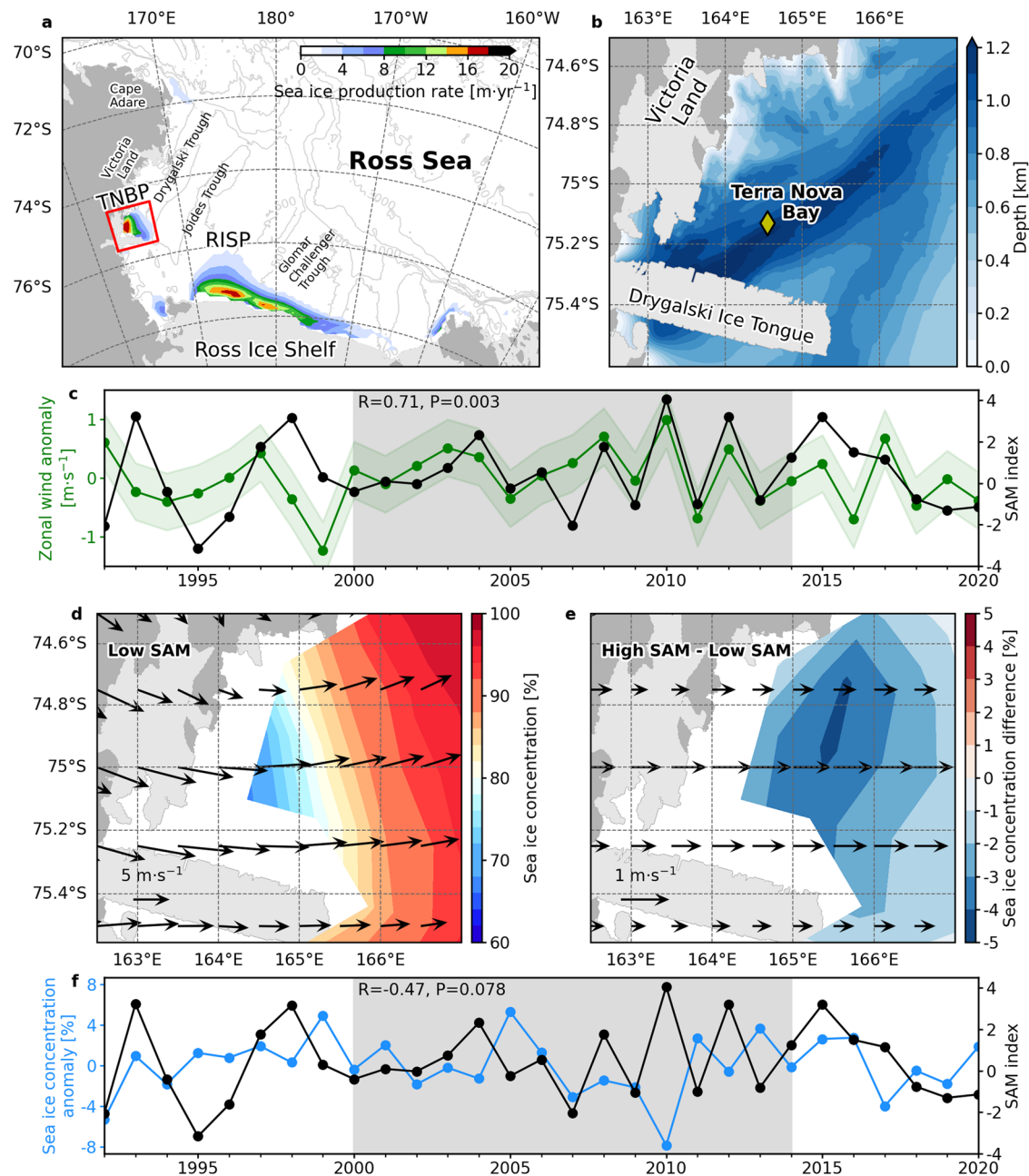


Fig. 1 | Relations of zonal wind and sea ice properties in the Terra Nova Bay polynya to the Southern Annular Mode (SAM). **a** Spatial distribution of annual cumulative sea ice production (unit: m) averaged over 1992–2013 in the Ross Sea. TNBP indicates the Terra Nova Bay polynya and RISIP indicates the Ross Ice Shelf polynya. **b** Bathymetry in the Terra Nova Bay. The yellow diamond indicates the location of the mooring used in this study. **c** Timeseries of anomalies of winter-mean 10-m zonal wind averaged over the Terra Nova Bay polynya and winter SAM index from 1992 to 2020; green shading indicates the standard deviation of wind anomaly. The coefficient (R) and p -value (P) of correlation between the two

timeseries are provided for the period 2000–2014. **d** Composite sea ice concentration and surface wind vectors over the Terra Nova Bay for low winter-SAM years in 2000–2014. **e** Differences in sea ice concentration and surface wind between high and low winter-SAM years in 2000–2014. **f** Timeseries of anomalies of winter-mean sea ice concentration averaged over the Terra Nova Bay polynya and winter SAM index from 1992 to 2020. The correlation coefficient (R) and p value (P) for these timeseries are provided for 2000–2014. Shading in (**c**) and (**f**) indicates the time period when significant correlation between zonal wind and winter SAM is detected (2000–2014).

sheets and the Transantarctic Mountains, synoptic-scale circulations and katabatic winds^{23,24}. Earlier studies revealed the variability of DSW formation in the TNBP and surrounding regions on synoptic to seasonal timescales^{16,25,26}, as well as the long-term trend of DSW salinity based on austral summer cruise observations^{27,28}. In fact, a dramatic seasonal salinity increase in bottom water, which is a clear indication of the start of DSW formation, occurs in austral winter²⁹. Up until now, there have been limited studies revealing the long-term variations of DSW formation and their connection to climate modes^{28,30}, and studies

discussing the relationship between wintertime DSW production and the dominant mode for climate variability in the southern hemisphere extratropical region—the Southern Annular Mode (SAM) are particularly scarce. Quantifying these interactions is essential to understanding the long-term variation of AABW and the meridional overturning circulation in the Southern Ocean.

SAM is characterized by opposing sea level pressure anomalies between the mid- and high-latitudes^{31–34}. A shift of SAM toward its positive phase is associated with strengthening and poleward

movement of the westerlies. While SAM plays a significant role in controlling infrequent opening of large-scale open-ocean sensible heat polynyas^{35,36}, its linkage to oceanic variability on interannual and decadal timescales in the coastal latent heat polynyas, which are important DSW formation sites, has not been previously studied. In this study, combining long-term satellite data, a 7-year mooring record for measuring DSW characteristics in the Southern Ocean, and numerical simulations from a high-resolution coupled ice-ocean model that reproduces DSW variability in the Ross Sea reasonably well, we find (1) that the interannual variability of wintertime sea ice production and DSW formation in the TNBP is modulated by SAM via changes in offshore winds, and in the RISB via surface air temperatures, (2) that the response of polynya processes to SAM affects the DSW volume on the slope and ultimately the AABW volume in the open ocean of the Pacific sector, and (3) that these relations have decadal variations that are influenced by the strength and location of the largest Antarctic climatological low pressure system—the Amundsen Sea Low (ASL).

Results

The relationship between interannual variations of wintertime atmospheric fields over the TNBP and SAM

While earlier work indicates that a shift toward the positive SAM phase can enhance westerly winds and may potentially affect the offshore winds over the TNBP³⁷, after examining the wind data from ERA5 and the SAM index over the past 30 years, we did not find a significant relationship between the interannual variations of zonal wind in this region and SAM (Fig. 1c) over the whole period. However, a significant and positive correlation between them is detected for the period 2000–2014 ($R = 0.71$, $P = 0.003$). In this period, the composite wind field for the 6 years with positive SAM (2003, 2004, 2008, 2010, 2012 and 2014) show notably stronger eastward (offshore) winds compared to that for the 9 years with negative SAM (2000, 2001, 2002, 2005, 2006, 2007, 2009, 2011 and 2013) (Fig. 1d, e), with the difference in average wind speed over the polynya being 0.6 m s^{-1} (10% of the mean winds, which is enough to significantly impact DSW formation rates³⁸). The winter mean surface air temperature, another atmospheric quantity that affects sea ice production in the polynya, was significantly and negatively correlated to the winter SAM ($R = -0.49$, $P = 0.007$; not shown) for the entire 1992–2020 period, while the correlation was weaker and insignificant for the period 2000–2014.

Mechanisms for a decadal relation between zonal winds over the TNBP and SAM

To find out why there exists a significant relationship between zonal wind over the TNBP and SAM for the period 2000–2014, we examined the role of other climate modes that can affect atmospheric circulations over the Ross Sea. Previous studies demonstrate that the ASL plays an important role in wind forcing over the this region^{39,40}. In particular, a deepening and westward movement of the ASL enhances southerlies from the Ross Ice Shelf and decreases air temperatures over the Ross Sea. While the ASL and SAM are found to be interrelated, with a deepening of the ASL often coinciding with a shift toward a positive SAM phase^{39,41}, they can also act as independent factors influencing the Ross Sea atmospheric circulations during different periods and seasons. For example, a significant correlation exists between the ASL longitude and SAM in austral autumn but not in other seasons⁴². An examination of the ASL indices reveals that from 2000, in austral winter, anomalies of the ASL central pressure relative to the climatological (1979–1999) mean remained positive until 2009 (Fig. 2a); a sharp decrease in pressure occurred in 2010, but the pressure rebounded quickly and oscillated around the climatological value between 2011–2014. Overall, comparing the period between 1979 and 1999 with that between 2000 and 2014, the ASL was

weakened and its extent was noticeably reduced (Fig. 2c, d), while SAM shifted slightly toward its positive phase as indicated by an increase of the period-mean SAM index by 0.2. These results suggest that the coincidence of a deeper ASL with positive SAM derived by previous studies may not be robust for all timescales, and that SAM and the ASL can be independent climate forcings for regional atmospheric circulations over some periods. In 2000–2014, the contraction of the ASL reduces its influence on the wind field over the western Ross Sea. In addition, we found that there was a dramatic eastward shift of the ASL center over the latter portion of 2000–2014 compared to the climatology (Fig. 2b). This would further weaken the influence of the ASL on the atmospheric forcing over the TNBP and can result in an enhanced relationship between winds in this region and other climate forcings such as SAM. This is consistent with past work which showed that during winter, SAM and the ASL zonal location are uncorrelated. In fact, a significant correlation is detected between the variations of meridional wind over the TNBP and the ASL central longitude during the period 1979–1999 ($R = -0.58$, $P = 0.001$; Fig. 2b), while such a relationship weakened during 2000–2014 ($R = 0.06$). The weakened correlation, along with the strong correlation of zonal wind to SAM during 2000–2014, suggests a competition between these two climate factors in controlling winds over the western Ross Sea, and that a weakening in the ASL influence enables a strengthened SAM impact in this region.

The connection between winter sea ice production in the TNBP and SAM

Between 2000–2014, under the enhanced offshore winds in positive SAM conditions that would favor the opening of the polynya, the winter sea ice concentration (SIC) in TNBP during high SAM years was lower than during low SAM years (Fig. 1d, e), with a difference in the polynya-average SIC value of 3% (some areas having differences of more than 5%), indicating an increased polynya extent. Similar to the zonal wind, the interannual variation of SIC was not significantly correlated with SAM for 1992–2020, but the correlation improves with SAM for 2000–2014 ($R = -0.47$) and is significant at the 90% confidence level (Fig. 1f). The correlations of interannual variations of SIC to zonal winds and air temperature are -0.80 ($P = 0.0003$) and 0.12 respectively, indicating that zonal winds are the major factor linking the SIC variability to SAM during 2000–2014 and that air temperatures do not play a significant role.

For the cumulative sea ice production (SIP) in June to August of each year during 2000–2013 available from satellite estimates, there was an overall trend of increasing SIP with increasing winter SAM (Fig. 3a–n). The average composite SIP in TNBP for the 6 high-SAM years is 0.7 m greater than that for the 9 low-SAM years. This period is also notable for a strong correlation between the interannual variations of winter SIP and SAM if data from 2007 are excluded ($R = 0.66$, $P = 0.03$; Fig. 3o), which year is featured by low SAM but not weak zonal wind and moderate SIC (Fig. 1c, f). In 2007, the density of cyclones that are centered near the Ross Ice Shelf reached the maximum between 2000 and 2014, and such cyclones can induce notable offshore wind over the TNBP region (Supplementary Fig. 1), which could have affected the relations between wind and SAM and between sea ice and SAM. Overall, the results above demonstrate that ice production was enhanced as strengthened offshore winds drove stronger offshore ice motion, enlarging the area for ocean-atmosphere heat losses to occur.

Enhancement in the DSW formation in positive SAM conditions in 2000–2014

Time series of the near-bottom salinity ($\sim 1050 \text{ m}$) from a mooring in the TNBP during freezing seasons (March to October) are shown for 7 years in 2000–2014, years when mooring data at consistent bottom depth are available (Fig. 4a–g). Earlier work suggested that while sea

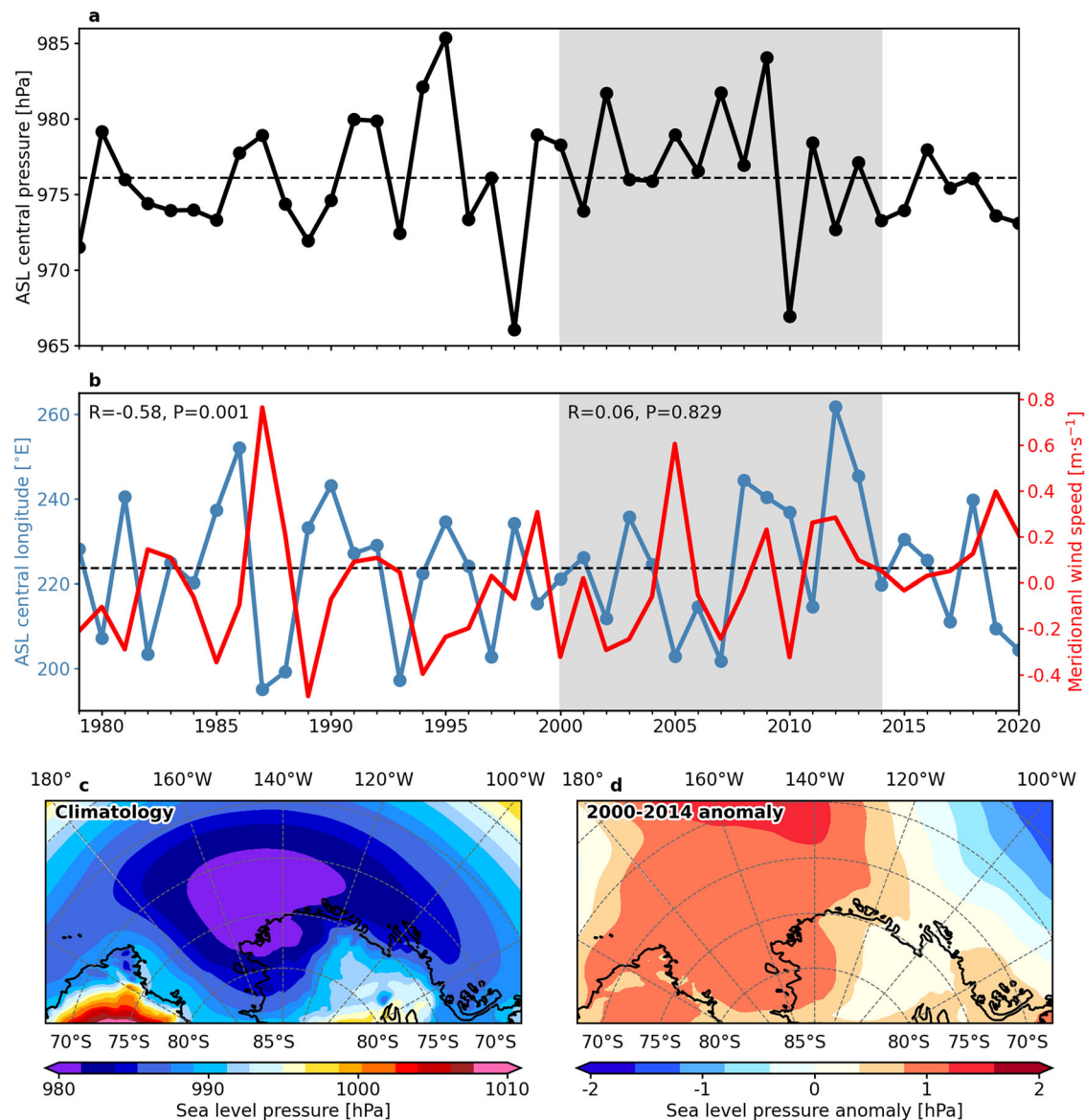


Fig. 2 | Changes in the Amundsen Sea Low between different periods. Time series of austral-winter mean (a) central pressure and (b) central longitude of the Amundsen Sea Low and meridional wind speed over the Terra Nova Bay between 1979 to 2020. Shading indicates the period 2000–2014. In (b), The correlation coefficients (R) and *p*-values (P) for the time series are provided separately for

1979–1999 and 2000–2014. **c** Austral-winter mean sea level pressure over the Pacific sector of the Southern Ocean averaged over 1979–1999 as the climatology. **d** Anomalies of austral-winter mean sea level pressure in 2000–2014 relative to the climatology.

ice production starts in early March in this region, significant increases in bottom salinity do not appear until mid-June and last until October²⁹. The late occurrence of salinity increase is possibly associated with advection of upstream ice shelf meltwater which decreases salinity in the TNBP area from March to July⁴³, as well the time it takes for the newly formed DSW to replenish the bottom layer as it is continuously exported out. We found that for some years (2008 and 2010) salinity increases did not appear until mid-July. We then calculated the salinity variations from mid-July to mid-October ($\Delta S_{Oct-Jul}$), i.e., the time period characterized by the strongest signal of salinity increase, and found that $\Delta S_{Oct-Jul}$ is positive (0.015–0.084) for all of the 4 years with positive SAM indices (2014, 2008, 2012 and 2010; Fig. 4h), and $\Delta S_{Oct-Jul}$ is negative or close to 0 (–0.036–0.004) in all of the 3 years with negative SAM indices (2009, 2011 and 2013). The interannual variation of $\Delta S_{Oct-Jul}$ has a significant, positive correlation with the variation of the winter SAM ($R = 0.83$, $P = 0.02$), and is significantly correlated with the interannual variability of winter SIP in TNBP in the

same period ($R = 0.81$, $P = 0.05$). The significant correlation to SAM also exists if we consider the salinity change for an extended period, from mid-June to the end of November ($R = 0.79$, $P = 0.04$). Such a correlation results from increased sea ice production and brine rejection during a positive SAM phase, which induces stronger ocean convection and increases the bottom salinity. As salinity is the major factor determining the variation of density in the polynya, the interannual variability of bottom potential density change from mid-July to mid-October ($\Delta \sigma_{Oct-Jul}$) is also significantly correlated with the winter SAM ($R = 0.83$, $P = 0.02$), indicating enhancement in the DSW formation during a positive SAM phase. Among the 7-year mooring data, hydrographic measurements at the middle of the water column (–500 m) are available for 5 years (2010, 2011, 2012, 2013, and 2014). The difference between potential density at the bottom and 500 m averaged over mid-July to mid-October, which indicates mean stratification during this period, was –0.04–0.02 kg m⁻³ for the 3 high-SAM years (2010, 2012, and 2014; Supplementary Fig. 2) and

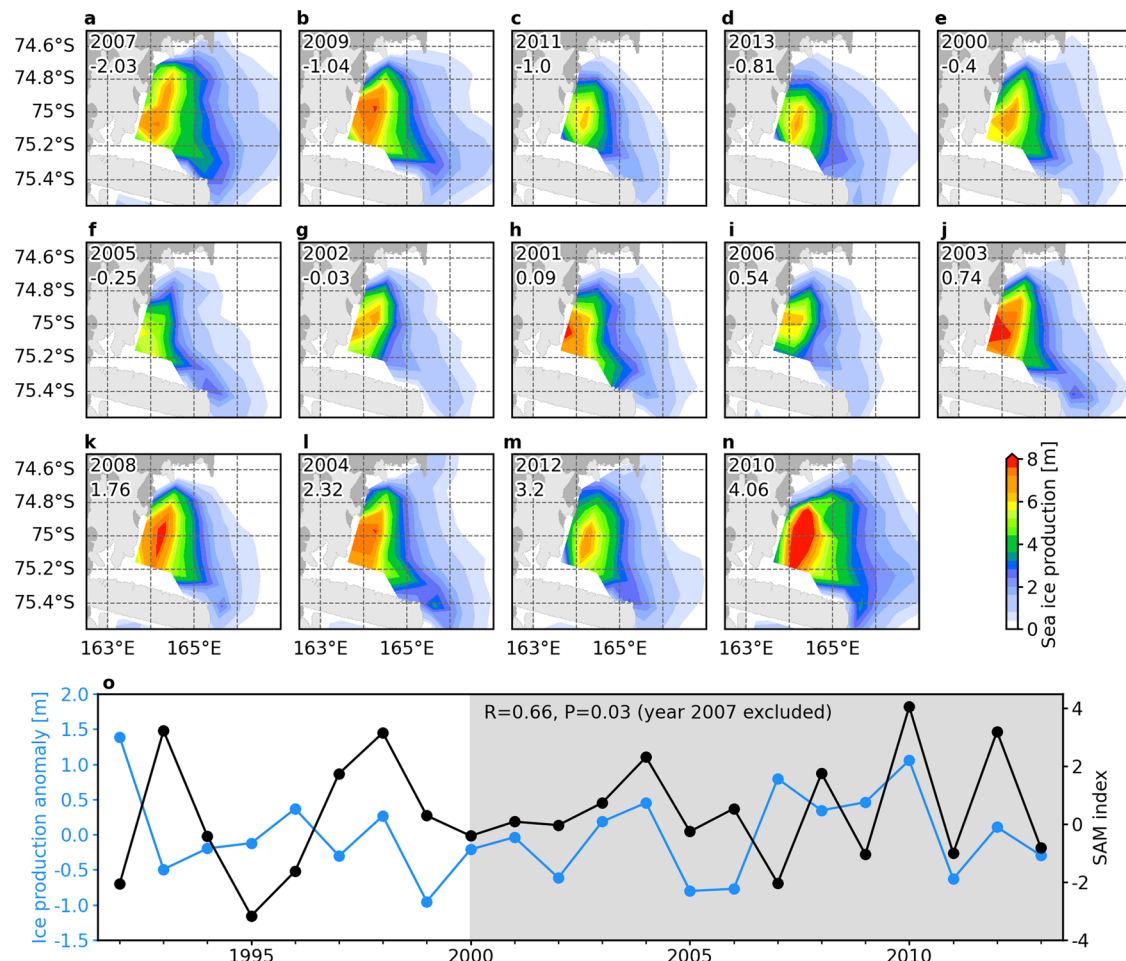


Fig. 3 | Link of sea ice production in the Terra Nova Bay polynya with the Southern Annular Mode (SAM). **a–n**, Cumulative sea ice production from June to August in each year of 2000–2013 over the Terra Nova Bay. The years are arranged in the order of increasing austral-winter SAM index, which is labeled in the upper

left corner of each panel. **o** Time series of cumulative sea ice production over winter and the winter SAM index. Shading indicates the time period when a significant correlation between the variations of sea ice production and SAM is detected.

0.04–0.05 kg m⁻³ for the 2 low-SAM years (2011 and 2013). This suggests weaker stratification and stronger convection in more positive SAM conditions that promote the DSW formation. The relationship of potential density change of bottom water with SAM is examined for a longer period, 2003–2014, using numerical simulations from a coupled high-resolution ocean-sea ice-ice shelf model that we developed for the Ross Sea and the Amundsen Sea, which can well capture the observed temporal variability of bottom water hydrography in the TNBP (see Methods). There exists significant correlation between the interannual variations of the modeled $\Delta\sigma_{Oct-Jul}$ and the winter SAM for this extended period, with $R=0.65$ and $P=0.02$ (Supplementary Fig. 3).

The response of DSW on the continental slope and AABW in the open ocean to the SAM variability

DSW formed in the TNBP is transported through the Drygalski Trough (Fig. 1a) toward the continental slope of the Ross Sea, where it mixes with Southern Ocean waters to form AABW that replenishes the Pacific sector and the Australian Antarctic Basin^{21,44}. As DSW mainly flows on the western side of troughs due to the Coriolis force⁴⁵, a box region at the slope abutting the western section of the Drygalski Trough (Fig. 5a) is selected to examine the potential linkage of DSW properties on the slope to the TNBP processes and SAM. Mooring observations in the Drygalski Trough just south of the box region reveal that a seasonal increase in the bottom water

neutral density starts in September and lasts until the following April^{46,47}, lagging the density change in the TNBP by a couple of months due to the water transport time. Given this fact, we computed the change of DSW (defined as neutral density greater than 28.27 kg m⁻³) layer thickness from early September of each year to the next April in the box region in 2003–2014 (Fig. 5a–l), using numerical simulations from the coupled ocean-sea ice-ice shelf model that can also well capture the bottom water characteristics on the Ross Sea slope (Methods). Compared to the DSW thickness changes in years with low SAM below or near 0, the changes in years with high SAM above 1.0 (in particular 2008, 2004 and 2010) are notably larger and can reach 80 m or above. Strong positive correlation exists between the interannual variations of DSW thickness change averaged over the box region and the density change $\Delta\sigma_{Oct-Jul}$ in the TNBP ($R=0.66$ and $P=0.05$; Fig. 5m). The relationship between interannual variations of DSW thickness change and winter SAM is also significant ($R=0.54$ and $P=0.07$; Fig. 5n). These results suggest that the variation of SAM can exert dramatic influence on the DSW volume in the slope area of the Ross Sea via changes in the coupled atmosphere-ice-ocean processes in the TNBP, which may potentially impact the AABW properties in the Pacific and Indian sectors of the Southern Ocean.

To verify the significant influence of the SAM variation on the DSW formation in the Ross Sea, including changes in both the TNBP and the Ross Ice Shelf polynya (RISP, Fig. 1a), and to further quantify

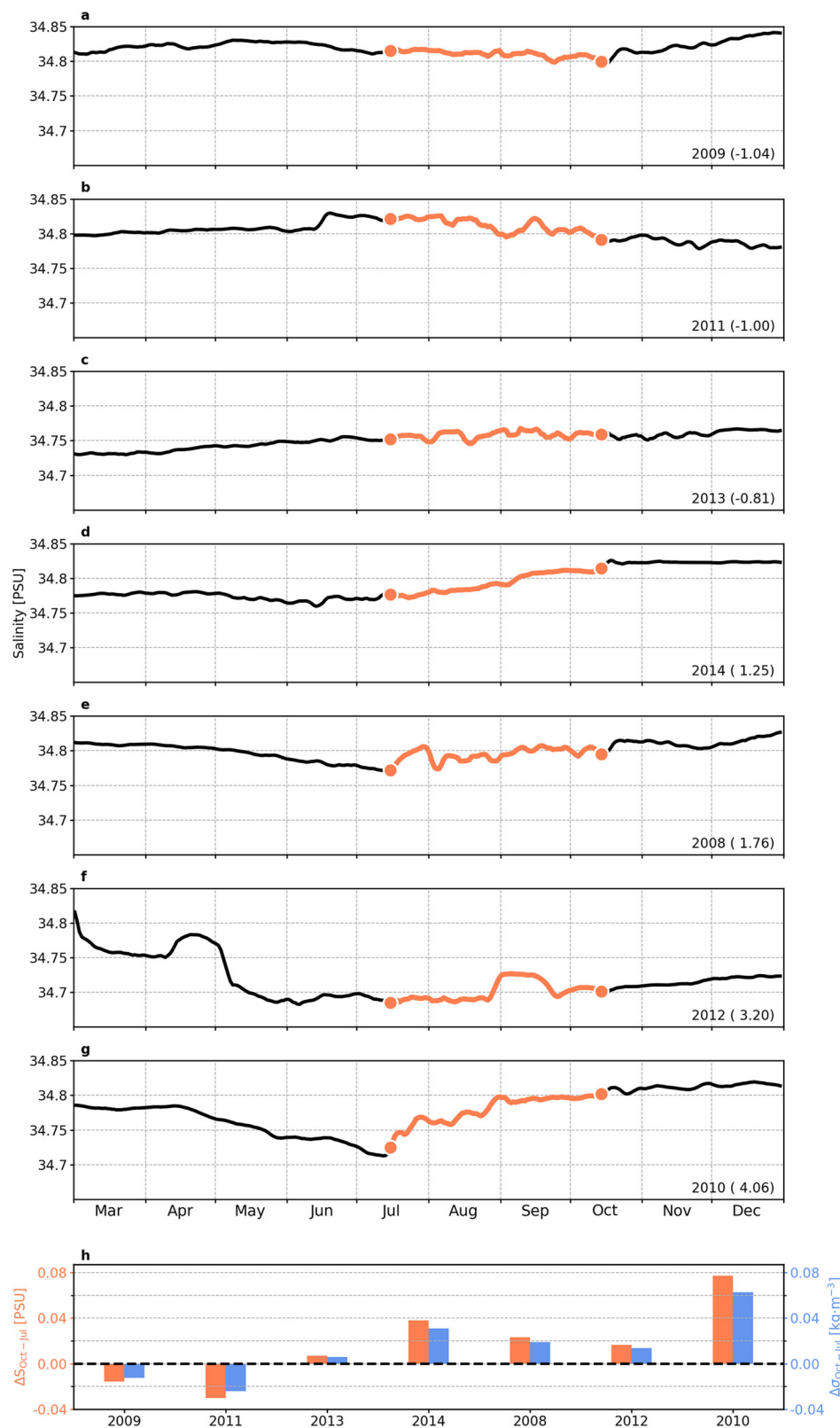


Fig. 4 | Relations of salinity and potential density changes in the bottom layer of the Terra Nova Bay polynya to the Southern Annular Mode (SAM). a–g Time series of daily-mean bottom (–1050 m) salinity obtained from Mooring D in the Terra Nova Bay from March to December between 2008–2014. The years are

arranged in the order of increasing austral-winter SAM index labeled in the lower right corner of each panel. **h** Changes in bottom salinity (ΔS) and bottom potential density ($\Delta \sigma$) from mid-July to mid-October in each year between 2008–2014. The years are arranged in the order of increasing austral-winter SAM index.

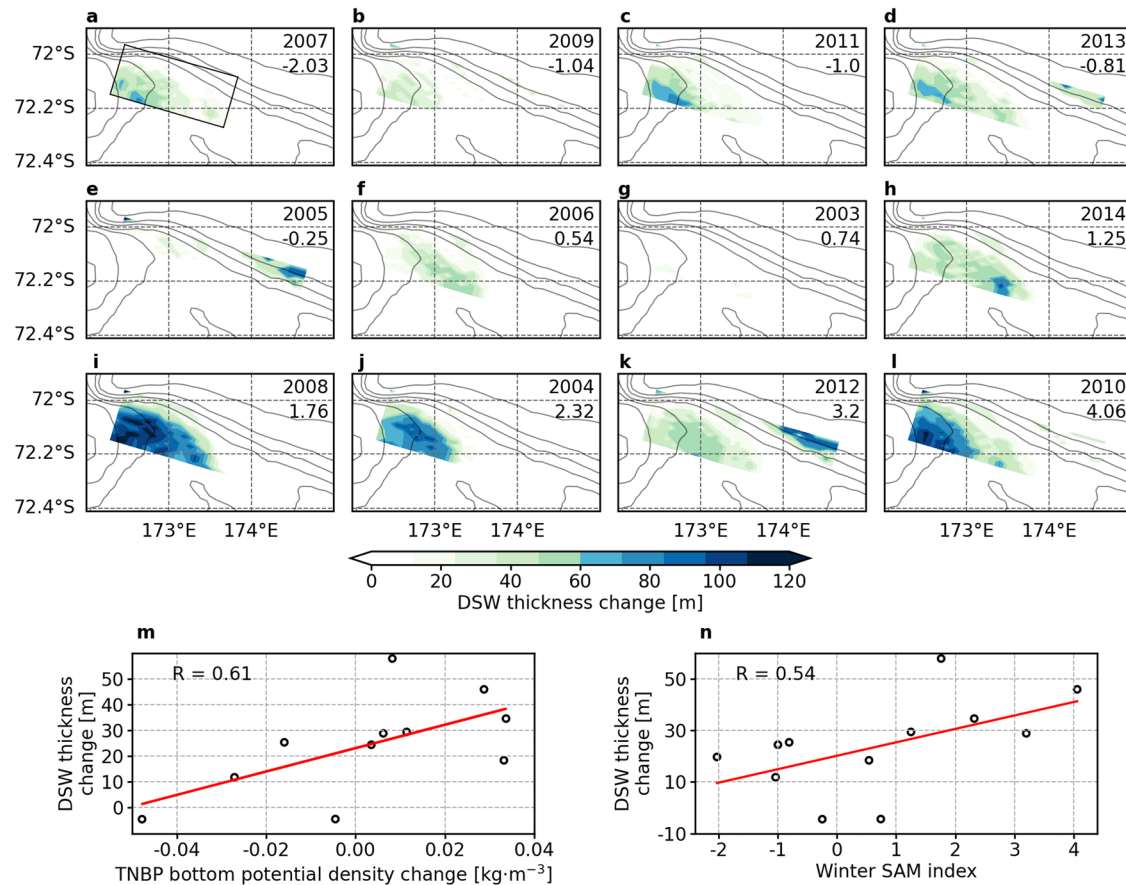


Fig. 5 | Response of the dense shelf water (DSW) thickness on the continental slope to the Southern Annular Mode (SAM). **a–l**, Changes of DSW thicknesses from early September to the next early April in the selected box region (indicated by the black box) on the Ross Sea slope near the Drygalski Trough in 2003–2014, which are obtained from model simulations. **a–l** are arranged in the order of

increasing austral-winter SAM index. **m** Regression between interannual variations of the DSW thickness change for the box region mean and the bottom potential density change ($\Delta\sigma_{Oct-Jul}$) in the Terra Nova Bay polynya from model simulations in 2003–2014. **n** Regression between interannual variations of the DSW thickness change for the box region mean and the austral-winter SAM index in 2003–2014.

the SAM-induced DSW changes as well as AABW changes in the open ocean, two numerical sensitivity experiments using the coupled ocean-sea ice-ice shelf model are conducted. In Experiments SAMP and SAMN, anomalies of atmospheric variables associated with one-standard-deviation (1-std) increase and 1-std decrease in the SAM index are added to the forcing fields of the realistic model simulation in 2003–2014 (named CTRL), respectively (see Methods). It can be seen that a shift toward the positive SAM phase can induce significant enhancement in the westerlies over most of the Ross Sea including the TNBP (Fig. 6a), and is also associated with decreases in surface air temperatures (SAT) over most of the Ross Sea that are most prominent near the Ross Ice Shelf (Fig. 6b), as a result of adiabatic cooling near the Antarctic continent²⁷. No significant changes in the meridional wind are found over the Ross Sea (not shown). The enhanced offshore wind over the TNBP and the cold air temperature over the RISP lead to increases in annual accumulative ice production (averaged over all simulation years) in these two polynyas in SAMP compared to CTRL (Fig. 6c), which can reach 1.0 m and above. Conversely, ice production in polynyas in SAMN is notably reduced compared to CTRL (Fig. 6d). The promotion and inhibition in ice production in SAMP and SAMN, respectively, result in increases and decreases of neutral density in the model bottom layer in the next February (the last month when DSW can be significantly affected by accumulative ice production from the previous freezing seasons, as new ice production begins in March) by more than 0.02 kg m^{-3} on the shelf and slope and more than 0.01 kg m^{-3} in the open ocean relative to those in CTRL (Fig. 6e, f). Ultimately, compared to CTRL, in SAMP

the DSW thicknesses increase by 20–50 m on the shelf and slope and the AABW thicknesses increase by 100–200 m in the open ocean of the Pacific sector (Fig. 6g), and in SAMN the thicknesses of DSW and AABW both show decreases (Fig. 6h). Compared to the role of offshore winds in polynya activity and the DSW formation, the role of SAT is discussed less often. In a model sensitivity experiment analyzing the effects of future climate change on the Ross Sea water masses, it is found that a decrease of SAT by 1°C over the Ross Sea will lead to a 7% increase of ice production over the shelf, 6% increase in the HSSW volume, and 9% increase in the HSSW flux off the Ross Sea shelf⁴⁸. To quantify the effects of SAT on the DSW formation in our study, sensitivity experiments were conducted in which SAT anomalies associated with a 1-std increase and decrease in SAM are added to the atmospheric forcing fields in a year with otherwise neutral SAM conditions. The results (Supplementary Fig. 4) show that the decrease of SAT during the positive SAM phase results in more DSW formation on the shelf (Supplementary Fig. 4b compared to 4a), and the increase in DSW thickness can reach 50 m and above, which is comparable to the increase of DSW thickness in Fig. 6g over the central and eastern Ross Sea that is mainly influenced by the RISP processes. These results further demonstrate that the effects of air temperature changes related to SAM on the RISP ice production and DSW production are significant.

Discussion

The mechanisms underlying the significant connection of ice production in polynyas of the Ross Sea and DSW formation with SAM in

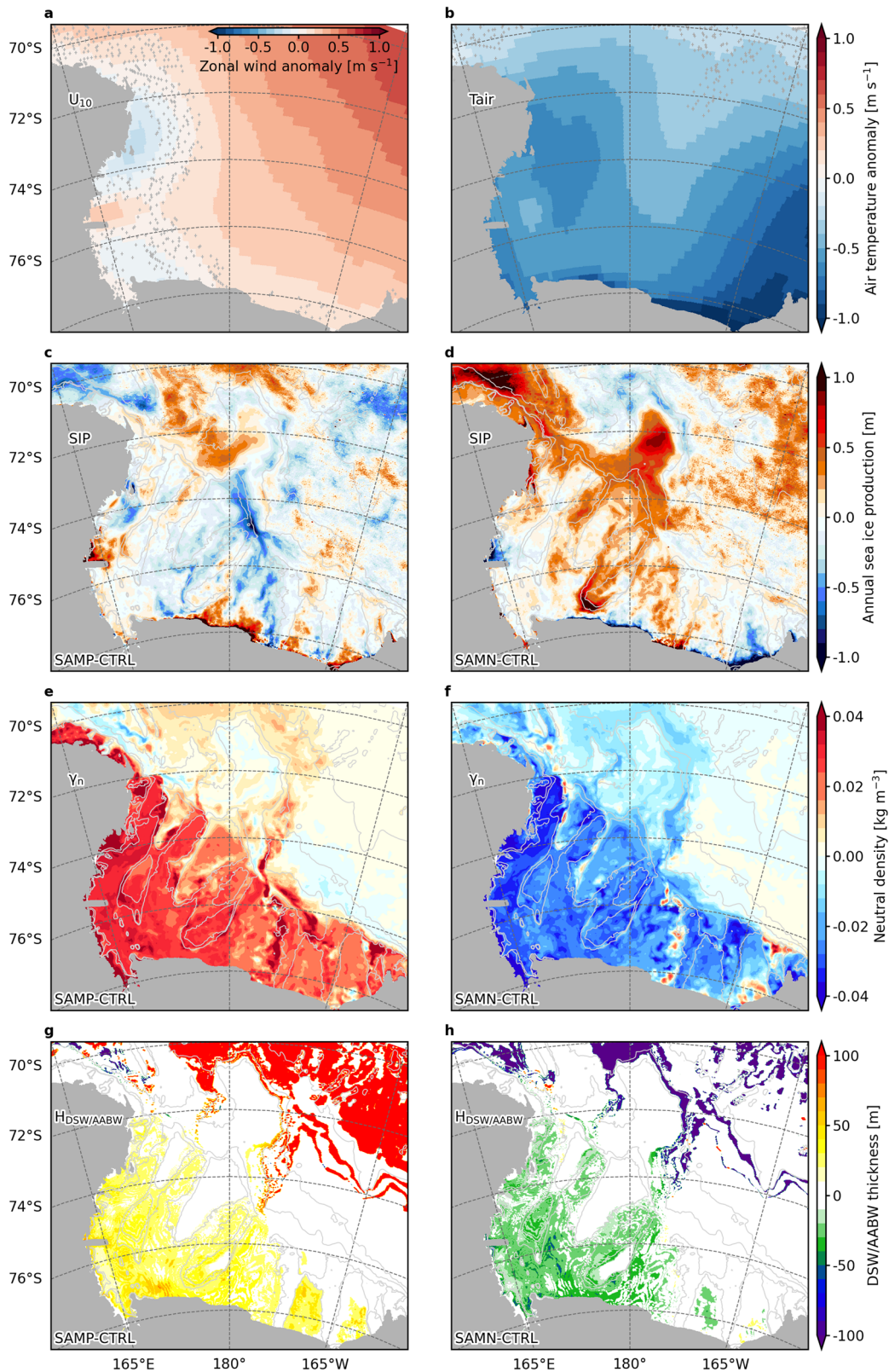


Fig. 6 | Results of numerical sensitivity experiments for shifts toward positive and negative phases of the Southern Annular Mode (SAM). Anomalies of (a) 10-m zonal wind and (b) surface air temperature over the Ross Sea associated with one-std-deviation increase in the SAM index. Crosses indicate areas where the anomalies are not significant at the 95% confidence level. Differences in annual accumulative (March–October) sea ice production averaged over years 2003–2013

(c) between SAMP and CTRL and (d) between SAMN and CTRL. Differences in neutral density in the bottom layer of the model in February averaged over years 2004–2014 (e) between SAMP and CTRL and (f) between SAMN and CTRL. Differences in thicknesses of DSW and AABW in February averaged over years 2004–2014 (g) between SAMP and CTRL and (h) between SAMN and CTRL.

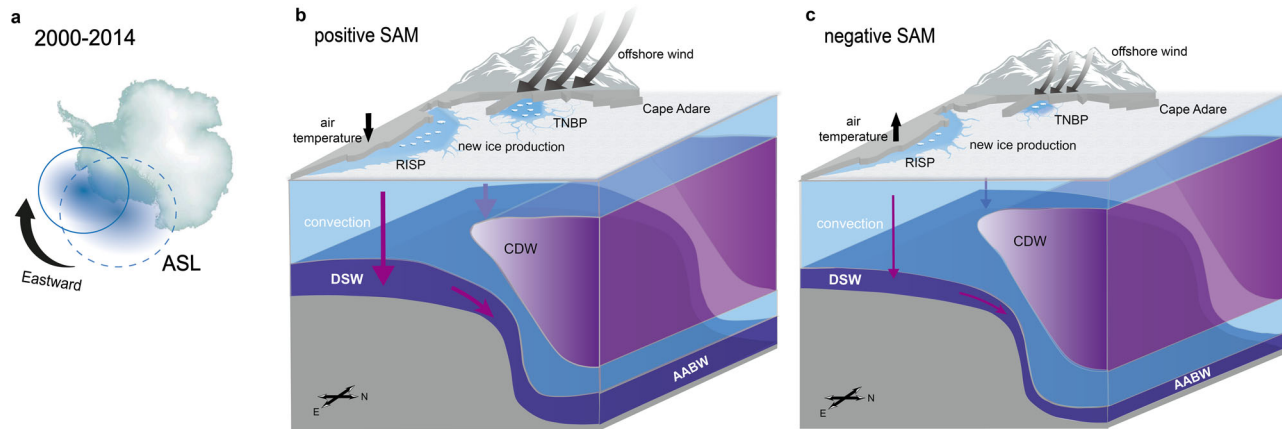


Fig. 7 | Schematic illustrating the impacts of the Southern Annular Mode (SAM) on the dense shelf water (DSW) formation in the Ross Sea in 2000–2014 and the physical mechanisms. In (a) 2000–2014, the Amundsen Sea Low moved eastward and became weaker, exerting less influence on the wind field over the western Ross Sea. SAM in turn dominates the interannual variability of wind. **b** The shift toward a positive SAM phase enhances the westerlies over the western Ross

Sea and decreases the surface air temperature, which promote sea ice production in the Terra Nova Bay Polynya (TNBP) and the Ross Ice Shelf polynya (RISP). Increased ice production enhances the DSW formation in the polynyas, finally leading to increased DSW volume on the continental shelf and slope and greater Antarctic Bottom Water (AABW) volume in the open ocean. The processes in (c) are opposite to those in (b) when SAM shifts toward its negative phase.

2000–2014 are illustrated in Fig. 7. Compared to the climatological condition, in 2000–2014 the ASL shifted eastward and was weaker (Fig. 7a), reducing its influence on the atmospheric fields over the Ross Sea³⁹. The eastward shift of the ASL may play a more important role in the western Ross Sea atmospheric circulation, as the variation of the ASL longitude is found to significantly correlate with wind over the TNBP in the period prior to 2000, while such correlation disappeared in 2000–2014. As a consequence of weakened impact of the ASL, SAM exerted more impacts and enhanced the westerly (offshore) wind over the TNBP during positive SAM phases (Fig. 7b), which promoted sea ice production and DSW formation in the polynya and subsequently increased the DSW volume in the shelf and slope areas. Decreased surface air temperatures over the Ross Sea in positive SAM conditions also favor more formation of sea ice and DSW in the RISP. The shift toward the positive SAM phase can ultimately increase the AABW volume in the open ocean off the Ross Sea. The opposite processes occur during a negative SAM phase (Fig. 7c). Projections of the ASL based on Coupled Model Intercomparison Project Phase 5 (CMIP5) and CMIP6 models^{49,50} both reveal that there is a trend of eastward shift of ASL in austral winter in the future. In addition, projections based on CMIP5 models show that under increasing greenhouse gas concentrations SAM will shift toward its positive phase by the end of this century⁵¹. Both the trends of ASL and SAM are expected to strengthen the dominance of SAM on atmospheric forcings over the Ross Sea and may result in more sea ice production in the polynyas, DSW formation on the shelf and slope and AABW volume in the open ocean. This may help weaken the observed freshening trend of bottom water in the Ross Sea⁵² and downstream in the Australian Antarctic Basin⁵³. It could also partially counteract potential reduction in the Ross Sea DSW salinity⁵⁴ and AABW production⁵⁵ resulting from projected increases in ice shelf melting in West Antarctica. It is worth noting that a positive shift of the SAM also leads to an intensification of CDW upwelling onto the shelf due to a poleward shift of the westerlies, causing warming of Antarctic shelf water and an increase in ice shelf melting rates^{56,57}, which can suppress DSW formation. This process is included in our sensitivity experiments as the SAM-induced atmospheric changes are applied over the entire model domain including the shelf and open ocean regions. The results of our study suggest that the effect of positive SAM on

enhancing DSW/AABW production via changes in sea-ice formation in polynyas overwhelms the effect of inhibiting the formation of these water masses via changes in shelf water temperature and ice shelf melting. A potential strengthened relation between DSW and SAM in the future allows the possibility of using projections of SAM from CMIP models, combined with our findings using a high-resolution regional model, to project changes in DSW and AABW in the Pacific sector of the Southern Ocean.

Methods

Atmospheric data

The atmospheric fields over the TNBP were derived from monthly data of the ERA5 reanalysis product. Surface winds at 10 m, air temperature at 2 m and the mean sea-level pressure are used. Comparisons between wind from ERA5 and wind from measurements at 6 automatic weather stations in the Ross Sea area show that the correlation coefficient between the variability of ERA5 wind speed and observed wind speed reaches 0.77 and above⁵⁸.

Sea ice concentration and production

SIC from satellite data is used to indicate the polynya extent in this work following earlier studies⁵⁹, as the retrieval of ice concentration does not depend on surface heat fluxes from reanalysis products as used in the retrieval of ice thickness and production. SIC data are taken from Version 2 of the Nimbus-7 SMMR and DMSP SSM/I-SSMIS Passive Microwave Data, available at the National Snow & Ice Data Center (NSIDC) with a horizontal resolution of 25 km. This dataset is generated from the brightness temperature data. Sea ice production data are obtained from heat- and salt-fluxes and the sea ice production analysis product is provided by the Institute of Low Temperature Science, Hokkaido University. Sea ice production is estimated by the heat flux calculation using thin-ice thickness (less than 0.2 m) derived from the SSM/I passive microwave data and atmospheric reanalysis products including ERA-40, ERA-interim and NCEP2⁶⁰. This dataset is available for 1992–2013.

Mooring observations

A mooring (mooring D) was deployed in the TNBP (75°06.10'S, 164°13.04'E) in February 1995 (Fig. 1b) by the MORsea Project of the Italian National Research Antarctic Program. The mooring was

recovered and re-deployed each year up to the present. The mooring was equipped with SBE16 temperature/conductivity recorders, Aanderaa RCM7/9 current meters, sediment traps and turbidity meters at different depths, and the depths varied over the years. We used data from the SBE16 recorders located near the ocean bottom (~50 m above the sea floor) from 2008 to 2014, a time span within the critical period of 2000–2014 when the SBE16 recorders were maintained at nearly the same depths. For analyzing the stratification, we also used data from the SBE16 recorders installed at the depth ~500 m from 2010 to 2014 and calculated the difference in potential density between the middle and bottom depths.

Climate indices

The seasonal SAM indices are provided by the British Antarctic Survey (<https://legacy.bas.ac.uk/met/gjma/sam.html>), which are calculated by the zonal pressure difference between the latitudes of 40 and 65°S based on station observations³¹. The ASL indices, including the central pressure and central longitude, are available at http://scotthosking.com/asl_index⁴⁹ as monthly data. These indices are derived from the ERA5 reanalysis product, and are temporally averaged to obtain the seasonal indices.

Numerical simulation data

In this study, we developed a high-resolution coupled ocean-sea ice-ice shelf model that covers the Ross Sea, the Amundsen Sea and the surrounding open ocean (see the model grids in Supplementary Fig. 5a). The model is an implementation of the Regional Ocean Modeling System (ROMS), which is a primitive-equation, finite-volume model with a terrain-following vertical coordinate system^{61,62}. The model horizontal resolution varies from ~2 km in the coastal areas to ~6 km in the open ocean, and over the TNBP area is 2–2.7 km. The model includes 32 vertical layers with variable thicknesses that depend on water column depth and are smaller at the surface and bottom. The model bathymetry and ice shelf draft are interpolated from BedMachine-Antarctica-v2.0, which has a spatial resolution of 500 m on the Antarctic Polar Stereographic projection. The sea ice module⁶³ is based on two-layer ice thermodynamics and a molecular sublayer beneath the sea ice^{64,65}, and elastic–viscous–plastic rheology for ice dynamics⁶⁶. A snow layer is included, and snow is converted into ice when the snow–ice interface is below sea level. The sea-ice model also includes a simple estimate of frazil ice production⁶⁷. The ice shelves in the model are static and there is no mass change of the ice shelf or iceberg calving. The thermodynamic and mechanical interactions between the ice shelf base and the water cavity underneath⁴⁷ are included as model processes. Vertical mixing of momentum and tracers are computed using the K-profile parameterization mixing scheme⁶⁸. Atmospheric forcing fields for the model are derived from the ERA5 reanalysis product. Temperature, salinity, sea surface height and depth-averaged velocity for the open boundaries are obtained from daily mean data of the Met Office Global Seasonal forecasting system version 5 (Glosea5)⁶⁹. Daily SIC boundary conditions are obtained from the Advanced Microwave Scanning Radiometer–Earth Observing System (AMSR-E) and Advanced Microwave Scanning Radiometer 2 (AMSR2) datasets provided by the University of Bremen using the ARTIST sea ice algorithm⁷⁰. Tidal forcing is derived from the global tidal solution TPXO9⁷¹. The model was initialized in January 1998 and integrated until April 2015; the simulations from 1998 to 2002 are treated as spin-up results. This model simulation is considered control experiment (CTRL) in this study.

The simulated accumulative sea ice production in austral winter are compared with satellite estimates in Supplementary Fig. 5. It can be seen that the model can well capture the SIP spatial patterns in the Ross Sea polynyas (a and b). The simulated sea ice production rates are higher than the satellite estimates. This may be partly due to inadequate representation of sea ice thermodynamic and

dynamic processes in the model, and partly due to the satellite estimates not including oceanic heat fluxes; such fluxes would increase the sea ice production based on observed vertical temperature profiles in the Terra Nova Bay¹³. The interannual variations of winter accumulative ice production from the model are significantly correlated with those from satellite estimates for both the TNBP (c) and RISP (not shown; $R = 0.52$ and $P = 0.1$). The simulated salinity in the TNBP is compared with mooring observations at the bottom and middle depths in Supplementary Fig. 6, and correlations between the modeled and observed salinity variations are significant for both depth levels. The simulated neutral density in the slope area of the Ross Sea is validated by bottom-water measurements from two moorings near Cape Adare (Supplementary Fig. 7), revealing significant correlations between the modeled and observed variations of bottom-water neutral density. The model is biased high for both salinity and density in the TNBP and slope regions, which could result from the overestimate of sea ice production and inadequate representation of ice shelf basal melting in the Amundsen Sea (about 140–190 Gt yr⁻¹ lower than satellite estimates) that leads to less fresh meltwater transported to the Ross Sea.

Numerical sensitivity experiments

Using monthly data of atmospheric forcing fields for the model and the SAM index in 2003–2014 and by performing linear regression, monthly anomalies of forcing variables including *u*- and *v*-component wind, surface air temperature, sea level pressure, humidity, precipitation and cloudiness associated with one-standard-deviation increase in the SAM index are derived. These anomalies are then added to and subtracted from the atmospheric forcing fields (repeated over all time steps in a month) of the CTRL simulation over the entire 2003–2014 period to perform the SAMP and SAMN experiments, respectively.

Statistical analysis

The relationship between two quantities is quantified by the Pearson correlation coefficient (*R*) and *p* value (*P*) that is determined by the Wald Test with *t*-distribution of the test statistic; $P \leq 0.1$ is considered statistically significant in this work. Composite analysis is performed to compare the patterns of winter surface wind and SIC over the TNBP under high- and low-SAM conditions in 2000–2014, and the composite fields are derived by averaging the quantities over 6 years with positive SAM indices and 9 years with negative SAM indices. Statistics for atmospheric variables and sea ice concentration for the TNBP are obtained over the region 75.4–74.6°S, 163–166°E.

Data availability

Atmospheric data are provided by the ECWMF ERA5 reanalysis product (<https://www.ecmwf.int/en/forecasts/datasets/reanalysis-datasets/era5>). Sea ice concentration data are obtained from Version 2 of the Nimbus-7 SMMR and DMSP SSM/I-SSMIS Passive Microwave Data available at the National Snow and Ice Data Center (<https://nsidc.org/data/nsidc-0051/versions/2>). Sea ice production data are archived at the website of the Institute of Low Temperature Science, Hokkaido University (<http://www.lowtem.hokudai.ac.jp/wwwod/polar-seaflux/>). Bottom water measurements from the two moorings near Cape Adare are collected by the Cape Adare Long-term Mooring (CALM) program (<https://www.marine-geo.org/tools/search/entry.php?id=NBPO801>). SAM indices are provided by the British Antarctic Survey (<https://legacy.bas.ac.uk/met/gjma/sam.html>) and the ASL indices are available at http://scotthosking.com/asl_index. Observational and model simulation data processed for making the display items in this manuscript are available at <https://doi.org/10.5281/zenodo.13702232>. Hydrographic data collected by the mooring in the Terra Nova Bay are available from the MORSea website (morsea.uniparthenope.it) upon request.

Code availability

The Python codes and scripts used to analyze the data and to generate the figures are archived and available at <https://doi.org/10.5281/zenodo.13671607>.

References

- Rintoul, S. R. On the origin and influence of Adélie Land bottom water. In *Ocean, Ice, and Atmosphere: Interactions at the Antarctic Continental Margin* Vol. 75, 151–171 (Wiley, 1998).
- Rintoul, S. R. Rapid freshening of Antarctic Bottom Water formed in the Indian and Pacific oceans. *Geophys. Res. Lett.* **34**, L06606 (2007).
- Jacobs, S. S. Bottom water production and its links with the thermohaline circulation. *Antarct. Sci.* **16**, 427–437 (2002).
- Williams, G. D. et al. Antarctic Bottom Water from the Adélie and George V Land coast, East Antarctica (140–149°E). *J. Geophys. Res. Ocean.* **115**, C04027 (2010).
- Ohshima, K. I. et al. Antarctic Bottom Water production by intense sea-ice formation in the Cape Darnley polynya. *Nat. Geosci.* **6**, 235–240 (2013).
- Orsi, A. H., Johnson, G. C. & Bullister, J. L. Circulation, mixing, and production of Antarctic Bottom Water. *Prog. Oceanogr.* **43**, 55–109 (1999).
- Lumpkin, R. & Speer, K. Global ocean meridional overturning. *J. Phys. Oceanogr.* **37**, 2550–2562 (2007).
- Johnson, G. C. Quantifying Antarctic Bottom Water and North Atlantic Deep Water volumes. *J. Geophys. Res. Ocean.* **113**, C05027 (2008).
- Arrigo, K. R. & van Dijken, G. L. Phytoplankton dynamics within 37 Antarctic coastal polynya systems. *J. Geophys. Res. Ocean.* **108**, 3271 (2003).
- Murakami, K. et al. Strong biological carbon uptake and carbonate chemistry associated with dense shelf water outflows in the Cape Darnley polynya, East Antarctica. *Mar. Chem.* **225**, 103842 (2020).
- Bromwich, D., Liu, Z., Rogers, A. N. & Van Woert, M. L. Winter atmospheric forcing of the Ross Sea Polynya. In *Ocean, ice and atmosphere, interactions at the Antarctic continental margin* Vol. 75, 101–133 (Wiley, 1998).
- Dale, E. R., McDonald, A. J., Coggins, J. H. J. & Rack, W. Atmospheric forcing of sea ice anomalies in the Ross Sea polynya region. *Cryosphere* **11**, 266–280 (2017).
- Thompson, L. et al. Frazil ice growth and production during katabatic wind events in the Ross Sea, Antarctica. *Cryosphere* **14**, 3329–3347 (2020).
- Farooq, U., Rack, W., McDonald, A. & Howell, S. Representation of sea ice regimes in the Western Ross Sea, Antarctica, based on satellite imagery and AMPS wind data. *Clim. Dyna.* **60**, 227–238 (2023).
- Nihashi, S. & Ohshima, K. I. Circumpolar mapping of Antarctic coastal polynyas and landfast sea ice: relationship and variability. *J. Clim.* **28**, 3650–3670 (2015).
- Tamura, T., Ohshima, K. I., Fraser, A. D. & Williams, G. D. Sea ice production variability in Antarctic coastal polynyas. *J. Geophys. Res. Ocean.* **121**, 2967–2979 (2016).
- Morales Maqueda, M. A., Willmott, A. J. & Biggs, N. R. T. Polynya dynamics: a review of observations and modeling. *Rev. Geophys.* **42**, RG1004 (2004).
- Visbeck, M. & Thurnherr, A. M. High-resolution velocity and hydrographic observations of the Drygalski Trough gravity plume. *Deep Sea Res. Part II Top. Stud. Oceanogr.* **56**, 835–842 (2009).
- Gordon, A. L. et al. Western Ross Sea continental slope gravity currents. *Deep Sea Res. Part II Top. Stud. Oceanogr.* **56**, 796–817 (2009).
- Meredith, M. P. Replenishing the abyss. *Nat. Geosci.* **6**, 166–167 (2013).
- Solodoch, A. et al. How does Antarctic Bottom Water cross the Southern Ocean? *Geophys. Res. Lett.* **49**, e2021GL097211 (2022).
- Orsi, A. H. & Wiederwohl, C. L. A recount of Ross Sea waters. *Deep Sea Res. Part II Top. Stud. Oceanogr.* **56**, 778–795 (2009).
- Parish, T. R., Cassano, J. J. & Seefeldt, M. W. Characteristics of the Ross Ice Shelf air stream as depicted in Antarctic Mesoscale Prediction System simulations. *J. Geophys. Res.* **111**, D12109 (2006).
- Coggins, J. H. J., McDonald, A. J. & Jolly, B. Synoptic climatology of the Ross Ice Shelf and Ross Sea region of Antarctica: k-means clustering and validation. *Int. J. Climatol.* **34**, 2330–2348 (2014).
- Yoon, S.-T. et al. Variability in high-salinity shelf water production in the Terra Nova Bay polynya. *Antarct. Ocean Sci.* **16**, 373–388 (2020).
- Le Bel, D. A., Zappa, C. J., Budillon, G. & Gordon, A. L. Salinity response to atmospheric forcing of the Terra Nova Bay polynya, Antarctica. *Antarct. Sci.* **33**, 318–331 (2021).
- Castagno, P. et al. Rebound of shelf water salinity in the Ross Sea. *Nat. Commun.* **10**, 5441 (2019).
- Silvano, A. et al. Recent recovery of Antarctic Bottom Water formation in the Ross Sea driven by climate anomalies. *Nat. Geosci.* **13**, 780–786 (2020).
- Rusciano, E., Budillon, G., Fusco, G. & Spezie, G. Evidence of atmosphere–sea ice–ocean coupling in the Terra Nova Bay polynya (Ross Sea–Antarctica). *Cont. Shelf Res.* **61**, 112–124 (2013).
- Zhou, S. et al. Slowdown of Antarctic Bottom Water export driven by climatic wind and sea-ice changes. *Nat. Clim. Chang.* **13**, 701–709 (2023).
- Marshall, G. J. Trends in the Southern Annular Mode from observations and reanalyses. *J. Clim.* **16**, 4134–4143 (2003).
- Sen Gupta, A. & England, M. H. Coupled ocean–atmosphere–ice response to variations in the Southern Annular Mode. *J. Clim.* **19**, 4457–4486 (2006).
- Zhang, Z. et al. Seasonal southern hemisphere multi-variable reflection of the southern annular mode in atmosphere and ocean reanalyses. *Clim. Dyn.* **50**, 1451–1470 (2018).
- Li, X. et al. Tropical teleconnection impacts on Antarctic climate changes. *Nat. Rev. Earth Environ.* **2**, 680–698 (2021).
- Gordon, A. L., Visbeck, M. & Comiso, J. C. A possible link between the Weddell Polynya and the Southern Annular Mode. *J. Clim.* **20**, 2558–2571 (2007).
- Campbell, E. C. et al. Antarctic offshore polynyas linked to Southern Hemisphere climate anomalies. *Nature* **570**, 319–325 (2019).
- Cheon, W. G., Cho, C.-B., Gordon, A. L., Kim, Y. H. & Park, Y.-G. The role of oscillating southern hemisphere westerly winds: Southern Ocean coastal and open-ocean polynyas. *J. Clim.* **31**, 1053–1073 (2018).
- Morrison, A. K. et al. Sensitivity of Antarctic shelf waters and abyssal overturning to local winds. *J. Clim.* **36**, 6465–6479.
- Coggins, J. H. J. & McDonald, A. J. The influence of the Amundsen Sea Low on the winds in the Ross Sea and surroundings: insights from a synoptic climatology. *J. Geophys. Res. Atmos.* **120**, 2167–2189 (2015).
- Raphael, M. N., Holland, M. M., Landrum, L. & Hobbs, W. R. Links between the Amundsen Sea Low and sea ice in the Ross Sea: seasonal and interannual relationships. *Clim. Dyna.* **52**, 2333–2349 (2019).
- Turner, J., Phillips, T., Hosking, J. S., Marshall, G. J. & Orr, A. The Amundsen sea low. *Int. J. Climatol.* **33**, 1818–1829 (2013).
- Clem, K., Renwick, J. A. & McGregor, J. Large-scale forcing of the Amundsen sea low and its influence on sea ice and West Antarctic temperature. *J. Clim.* **30**, 8405–8424 (2017).
- Yan, L. et al. The salinity budget of the Ross Sea continental shelf, Antarctica. *J. Geophys. Res. Ocean* **128**, e2022JC018979 (2023).
- Kusahara, K., Williams, G. D., Tamura, T., Massom, R. & Hasumi, H. Dense shelf water spreading from Antarctic coastal polynyas to the

- deep Southern Ocean: a regional circumpolar model study. *J. Geophys. Res. Ocean.* **122**, 6238–6253 (2017).
45. Morrison, A. K., McC. Hogg, A., England, M. H. & Spence, P. Warm Circumpolar Deep Water transport toward Antarctica driven by local dense water export in canyons. *Sci. Adv.* **6**, 1–10 (2020).
46. Castagno, P., Falco, P., Dinniman, M. S., Spezie, G. & Budillon, G. Temporal variability of the Circumpolar Deep Water inflow onto the Ross Sea continental shelf. *J. Mar. Syst.* **166**, 37–49 (2017).
47. Bowen, M. M. et al. The role of tides in bottom water export from the western Ross Sea. *Sci. Rep.* **11**, 2246 (2021).
48. Dinniman, M. S., Klinck, J. M., Hofmann, E. E. & Smith, W. O. Jr. Effects of projected changes in wind, atmospheric temperature, and freshwater inflow on the Ross Sea. *J. Clim.* **31**, 1619–1635 (2018).
49. Hosking, J. S., Orr, A., Bracegirdle, T. J. & Turner, J. Future circulation changes off West Antarctica: sensitivity of the Amundsen Sea Low to projected anthropogenic forcing. *Geophys. Res. Lett.* **43**, 367–376 (2016).
50. Gao, M. et al. Historical fidelity and future change of Amundsen Sea Low under 1.5 °C–4 °C global warming in CMIP6. *Atmos. Res.* **255**, 105533 (2021).
51. Zheng, F., Li, J., Clark, R. T. & Nnamchi, H. C. Simulation and projection of the southern hemisphere annular mode in CMIP5 models. *J. Clim.* **26**, 9860–9879 (2013).
52. Jacobs, S. S., Giulivi, C. F. & Dutrieux, P. Persistent Ross Sea freshening from imbalance West Antarctic ice shelf melting. *J. Geophys. Res. Ocean.* **127**, 1–19 (2022).
53. Gunn, K. L., Rintoul, S. R., England, M. H. & Bowen, M. M. Recent reduced abyssal overturning and ventilation in the Australian Antarctic Basin. *Nat. Clim. Chang.* **13**, 537–544 (2023).
54. Moorman, R., Morrison, A. K. & McC. Hogg, A. Thermal responses to Antarctic ice shelf melt in an eddy-rich global ocean–sea ice model. *J. Clim.* **33**, 6599–6620 (2020).
55. Li, Q. et al. Abyssal ocean overturning slowdown and warming driven by Antarctic meltwater. *Nature* **615**, 841–847 (2023).
56. Purich, A. & England, M. H. Historical and future projected warming of Antarctic shelf bottom water in CMIP6 models. *Geophys. Res. Lett.* **48**, e2021GL092752 (2021).
57. Naughten, K. A. et al. Future projections of Antarctic ice shelf melting based on CMIP5 scenarios. *J. Clim.* **31**, 5243–5261 (2018).
58. Xie, C., Zhang, Z. & Zhou, M. Effects of SAM and ENSO on winter climate over the Ross Sea and the Amundsen Sea. *Chin. J. Pol. Res.* **35**, 167–182 (2023).
59. Wenta, M. & Cassano, J. J. The atmospheric boundary layer and surface conditions during katabatic wind events over the Terra Nova Bay Polynya. *Remote Sens.* **12**, 4160 (2020).
60. Tamura, T., Ohshima, K. I. & Nihashi, S. Mapping of sea ice production for Antarctic coastal polynyas. *Geophys. Res. Lett.* **35**, L07606 (2008).
61. Haidvogel, D. B. et al. Ocean forecasting in terrain-following coordinates: formulation and skill assessment of the Regional Ocean Modeling System. *J. Comput. Phys.* **227**, 3595–3624 (2008).
62. Shchepetkin, A. F. & McWilliams, J. C. Correction and commentary for “Ocean forecasting in terrain-following coordinates: formulation and skill assessment of the regional ocean modeling system” by Haidvogel et al., *J. Comp. Phys.* **227**, pp. 3595–3624. *J. Comput. Phys.* **228**, 8985–9000 (2009).
63. Budgell, W. P. Numerical simulation of ice-ocean variability in the Barents Sea region. *Ocean Dyn.* **55**, 370–387 (2005).
64. Mellor, G. L. & Kantha, L. An ice-ocean coupled model. *J. Geophys. Res. Ocean.* **94**, 10937–10954 (1989).
65. Häkkinen, S. & Mellor, G. L. Modeling the seasonal variability of a coupled Arctic ice-ocean system. *J. Geophys. Res. Ocean.* **97**, 20285–20304 (1992).
66. Hunke, E. C. & Dukowicz, J. K. An elastic–viscous–plastic model for sea ice dynamics. *J. Phys. Oceanogr.* **27**, 1849–1867 (1997).
67. Steele, M., Mellor, G. L. & McPhee, M. G. Role of the molecular sublayer in the melting or freezing of sea ice. *J. Phys. Oceanogr.* **19**, 139–147 (1989).
68. Large, W. G., McWilliams, J. C. & Doney, S. C. Oceanic vertical mixing: a review and a model with a nonlocal boundary layer parameterization. *Rev. Geophys.* **32**, 363–403 (1994).
69. Maclachlan, C. et al. Global Seasonal forecast system version 5 (GloSea5): a high-resolution seasonal forecast system. *Q. J. R. Meteorol. Soc.* **141**, 1072–1084 (2015).
70. Spreen, G., Kaleschke, L. & Heygster, G. Sea ice remote sensing using AMSR-E 89-GHz channels. *J. Geophys. Res.* **113**, C02S03 (2008).
71. Egbert, G. D. & Erofeeva, S. Y. Efficient inverse modeling of barotropic ocean tides. *J. Atmos. Ocean. Technol.* **19**, 183–204 (2002).

Acknowledgements

This study is funded by the Key Research & Development Program of the Ministry of Science and Technology of China (Grant No. 2022YFC2807601), the National Natural Science Foundation of China (Grant No. 41941008), and the Shanghai Science and Technology Committee (Grant No. 20230711100 and Grant No. 21QA1404300). M.H.E. acknowledges funding from the Australian Research Council (SR200100008 and DP190100494). A.S. acknowledges funding from NERC (NE/V014285/1). We acknowledge the support from the Shanghai Pilot Program for Basic Research—Shanghai Jiao Tong University (Grant no. TQ1400201) and the Shanghai Frontiers Science Center of Polar (SCOPS). The mooring data were collected as part of the MORSea project, which was financially and logistically supported by the Italian National Programme for Antarctic Research (PNRA).

Author contributions

Z.Z. conceived this study, analyzed the observational data, designed the numerical model configurations and analyzed the numerical results. C.X. conducted the numerical simulations and sensitivity experiments and analyzed the simulation results. P.C. and G.B. collected part of the mooring data. M.H.E., M.S.D. and A.S. contributed to the design of sensitivity numerical experiments. X.W. and C.W. participated in part of data processing. L.Z., X.L. and M.Z. provided insights into the interpretation of the results. Z.Z. wrote the manuscript with input from all the co-authors.

Competing interests

The authors declare no competing interests.

Additional information

Supplementary information The online version contains supplementary material available at <https://doi.org/10.1038/s41467-024-52524-x>.

Correspondence and requests for materials should be addressed to Zhaoru Zhang.

Peer review information *Nature Communications* thanks Guijun Guo, Adrian McDonald, and the other, anonymous, reviewer for their contribution to the peer review of this work. A peer review file is available.

Reprints and permissions information is available at <http://www.nature.com/reprints>

Publisher's note Springer Nature remains neutral with regard to jurisdictional claims in published maps and institutional affiliations.

Open Access This article is licensed under a Creative Commons Attribution-NonCommercial-NoDerivatives 4.0 International License, which permits any non-commercial use, sharing, distribution and reproduction in any medium or format, as long as you give appropriate credit to the original author(s) and the source, provide a link to the Creative Commons licence, and indicate if you modified the licensed material. You do not have permission under this licence to share adapted material derived from this article or parts of it. The images or other third party material in this article are included in the article's Creative Commons licence, unless indicated otherwise in a credit line to the material. If material is not included in the article's Creative Commons licence and your intended use is not permitted by statutory regulation or exceeds the permitted use, you will need to obtain permission directly from the copyright holder. To view a copy of this licence, visit <http://creativecommons.org/licenses/by-nc-nd/4.0/>.

© The Author(s) 2024